HHS Public Access

Author manuscript

Hepatology. Author manuscript; available in PMC 2020 April 01.

Published in final edited form as:

Hepatology. 2019 April ; 69(4): 1535–1548. doi:10.1002/hep.30364.

Cannabinoid-1 Receptor Antagonism Improves Glycemic Control and Increases Energy Expenditure via Sirt1/mTORC2 and AMPK Signaling

Jie Liu, **Grzegorz Godlewski**, **Tony Jourdan**, **Ziyi Liu**, **Resat Cinar**, **Keming Xiong**, and **George Kunos**

Laboratory of Physiologic Studies, National Institute on Alcohol Abuse and Alcoholism, National Institutes of Health, Bethesda, MD 20892

Abstract

Endocannabinoids promote energy conservation in obesity, whereas cannabinoid-1 receptor (CB_1R) blockade reverses body weight gain and insulin resistance and increases energy expenditure. Here we investigated the molecular mechanisms of the catabolic effects of CB_1R blockade in the liver. Exposure of primary mouse hepatocytes and HepG2 cells to the CB_1R agonist ACEA inhibited the expression of Sirt1 and Rictor, a component of mTORC2, and suppressed insulin-induced Akt phosphorylation at ser473. These effects were reversed by peripheral CB_1R antagonist JD5037 in control hepatocytes but not in hepatocytes deficient in Sirt1 and/or Rictor, indicating that these two proteins are required for the CB_1R-mediated inhibition of insulin signaling. Feeding C57BL/6J mice a high-fat diet (HFD) inhibited hepatic Sirt1/mTORC2/Akt signaling, and the inhibition was reversed by rimonabant or JD5037 in wild-type but not liver-specific $Sirt1^{-/-}$ (Sirt1-LKO) mice, to levels observed in hepatocyte-specific $CB_1R^{-/-}$ ($LCB_1R^{-/-}$) mice. A similar attenuation of hyperglycemia and hyperinsulinemia in obese wild-type but not Sirt1-LKO mice could be attributed to insufficient reversal of HFD-induced mitochondrial ROS generation in peripheral tissues in the latter. In contrast, JD5037 treatment was equally effective in HFD-fed wild-type and Sirt1-LKO mice in reducing hepatic steatosis, increasing fatty acid β-oxidation and activating AMPK via LKB1, resulting in a similar increase in total energy expenditure in the two strains. ***Conclusion:*** peripheral CB_1R blockade in obese mice improves glycemic control via the hepatic Sirt1/mTORC2/Akt pathway, whereas it increases fatty acid oxidation via LKB1/AMPK signaling.

The endocannabinoid (EC) system becomes overactive in obesity/metabolic syndrome, resulting in increased energy intake and decreased energy expenditure. Activation of CB_1R promotes food intake (1), increases lipogenesis in white adipocytes (2) and liver (3) by maximizing *de novo* lipogenesis and triglyceride accumulation and minimizing lipolysis and fatty acid oxidation, and also impairs leptin signaling and hepatic insulin action (4). Blockade of CB_1R reverses these effects, as documented in DIO mice (5) and in humans with the metabolic syndrome (6). However, neuropsychiatric side effects due to blockade of

Correspondence: jiel@mail.nih.gov or george.kunos@nih.gov.

Conflicts of interest

The authors declare no conflicts.

CB_1R in the CNS preclude the therapeutic use of globally acting CB_1R antagonists. Peripherally restricted CB_1R antagonists were recently found to reverse obesity and its metabolic complications without causing behavioral effects or occupying CB_1R in the CNS (7–10). Thus, the mechanism involved in the antiobesity effects of CB_1R blockade can be triggered at peripheral sites.

The mechanistic target of rapamycin (mTOR) signaling pathway is an energy and nutrient sensor that regulates cellular processes involved in energy homeostasis. mTOR is an atypical serine/threonine protein kinase which interacts with two scaffold proteins, Raptor and Rictor, to form two distinct complexes named mTORC1 and mTORC2, which are key regulators of cell growth, survival and proliferation (11). mTORC2 primarily functions as an effector of insulin/PI3K signaling, phosphorylates Akt at its hydrophobic Ser473 site, which primes its further phosphorylation at Thr308 for a full activation (12). Studies using liver-specific Rictor-deleted mice demonstrated that mTORC2 is required for insulin-mediated lipogenesis and suppression of hepatic glucose production (13).

Sirtuin-1 (Sirt1), a nuclear NAD+-dependent protein deacetylase, promotes Rictor expression and downstream phosphorylation of Akt at ser473, which suppresses gluconeogenesis via phosphorylation of FOXO1 (14). The metabolic shift from carbohydrate to fat utilization may reduce reactive oxygen species (ROS) production and extend life span (15).

Another fuel-sensing molecule, the AMP-activated protein kinase (AMPK), controls lipid metabolism via phosphorylation of acetyl coenzyme A carboxylase-1 (ACC1), ACC2 (16), and Srebp1 (17). Activation of AMPK in the liver therefore results in decreased fatty-acid, triglyceride and sterol synthesis, and increased fatty-acid oxidation (18). Activation of CB_1R in the liver inhibits AMPK activity (19), whereas the globally acting CB_1R inverse agonist rimonabant decreases lipogenesis through activation of AMPK, which reduces liver X receptor α (LXRα)-mediated Srebp1 expression via the cAMP-dependent protein kinase A (PKA)/liver kinase B1 (LKB1) axis downstream of $Ga_{i/o}$ inhibition (20). Rimonabant also increases mitochondrial function through decreasing malonyl CoA (21) and increasing mitochondrial oxygen consumption and fatty-acid β-oxidation (22, 23).

Although insulin sensitization by CB_1R blockade phenocopies the effects of mTORC2 signaling, a link between the two systems at the cellular level has not yet been explored. The findings presented here demonstrate that blockade of peripheral CB_1R improves insulin sensitivity and glycemic control via Sirt1/mTORC2 signaling, whereas its effect on promoting energy expenditure by increasing fatty acid oxidation is independent of hepatic Sirt1 and involves AMPK activation.

Materials and Methods

MICE

Genetically modified strains backcrossed 10 times to a C57BL/6J background were bred from heterozygote pairs to allow for the use of littermate controls. All animal experiments were approved by the institutional animal care and use committee. Hepatic $CB_1R^{-/-}$

($LCB1^{-/-}$) mice (24) and liver-specific $Sirt1^{-/-}$ (Sirt1-LKO) mice were generated as described (25). Eight-week-old mice were placed on standard chow (STD; NIH-31 rodent diet) or a high-fat diet (HFD, TD97070; Harlan Teklad, Frederick, MD) containing 33.5% fat (60% of calories) 26.5% carbohydrate, and 27.4% protein for 18 weeks before daily treatment with vehicle, rimonabant 5mg/kg i.p., or JD5037 3mg/kg by oral gavage for an additional 2 or 4 weeks, as indicated.

DRUGS

JD5037 was obtained from Jenrin Discovery (26). Rimonabant was from the National Institute of Drug Abuse Drug Supply Program. Arachidonyl-2'-chloroethylamide (ACEA) was from Tocris (Minneapolis, MN). EX-527 was purchased from Sigma (St. Louis, MO).

PRIMARY MOUSE HEPATOCYTES

C57BL6J mice were anesthetized with sodium pentobarbital (30 mg/kg i.p.), and the portal vein was cannulated under aseptic conditions. The liver was first perfused with EGTA solution (5.4 mmol/L KCl, 0.44 mmol/L KH_2PO_4, 140 mmol/L NaCl, 0.34 mmol/L $Na_2HPO_4$0.5 mmol/L EGTA, and 25 mmol/L Tricine, pH 7.2) and DMEM and digested with DMEM containing 0.075% type I collagenase (Sigma, St. Louis, MO). Isolated hepatocytes were then cultured at 60–70% confluence in DMEM containing 10% FBS in rat-tail collagen-coated plates. After removing unattached cells, adherent hepatocytes were then treated with CB_1R agonist and/or antagonist for the indicated time period before harvesting for further analysis. HepG2 cells were maintained in DMEM medium containing 10% FBS (ATCC, Manassas, VA) and were treated similarly as primary mouse hepatocytes.

CELL TREATMENT AND GENE KNOCKDOWN

Mouse primary hepatocytes or HepG2 cells were transfected with scrambled siRNA, Sirt1-siRNA, Rictor-siRNA or LKB1-siRNA (GE Dharmacon, Lafayette, CO) for 24h. Cells were then treated with DMSO or JD5037 100nM with or without 1μM ACEA overnight, followed by 100nM insulin for 15 minutes. SiRNA transfection was performed with Lipofectamine RNAiMAX (Invitrogen, Gaithersburg, MD). The Sirt1 inhibitor EX-527 50μM was added 1h before the addition of JD5037 or rimonabant for 4h. For fatty acid oxidation assay, cells were treated with 100 nM rimonabant or JD5037 for 10 min and the assay was performed as indicated in the manufacturer's instructions (Abcam, Cambridge, MA).

Details on the pyruvate tolerance test, hyperinsulinemic/euglycemic clamp and 2-deoxyglucose uptake, serum insulin measurements, hepatic fatty acid profile and liver triglyceride measurements, qRT-PCR, Western blotting and immunoprecipitation, SIRT1 activity and fatty acid oxidation assays, mitochondria complex activity and indirect calorimetry measurements are provided on line as Supplementary Methods.

STATISTICAL ANALYSES

Values are expressed as mean ± standard error (SEM). Significant differences were tested using two-tailed, unpaired Student's t test, and among more than two groups by analysis of one-way ANOVA. Differences were considered significant at $P<0.05$.

Results

ACTIVATION OF CB_1R INHIBITS SIRT1/MTORC2 SIGNALING IN MOUSE PRIMARY HEPATOCYTES AND HEPG2 CELLS

Activation of hepatic CB_1R impairs insulin signaling via decreased Akt phosphorylation, resulting in hepatic insulin resistance and elevated blood glucose (4), and mTORC2 is required for the insulin-mediated suppression of hepatic gluconeogenesis (27). Because Sirt1 promotes the transcription of the gene encoding Rictor, which triggers phosphorylation of Akt at ser473 and suppresses gluconeogenesis through phosphorylation of FOXO1 (14), we explored the involvement of Sirt1 and Rictor in the CB_1R-inhibition of Akt phosphorylation. In mouse primary hepatocytes, the CB_1R agonist 2-arachidonyl chloroethylamine (ACEA) caused rapid and sustained reductions in *Sirt1* and *Rictor* mRNA, which paralleled decreases in their protein levels (Fig. 1A, B), and both effects were prevented by JD5037 (Fig. 1A). Rimonabant or JD5037 alone increased Rictor levels, which was blocked by the Sirt1 inhibitor EX-527 (Fig. 1C). These findings suggest that activation of hepatic CB_1R inhibits *Sirt1* and *Rictor* expression, whereas CB_1R inverse agonism does the opposite. To address the role of Sirt1 and Rictor in CB_1R inhibition of hepatic insulin signaling, we tested the effect of their siRNA-mediated knockdown on CB_1R modulation of insulin-induced Akt phosphorylation in mouse primary hepatocytes. Treatment of mock-transfected cells with 100 nM insulin for 15 min induced Akt phosphorylation at ser473, which was inhibited by 1 μM ACEA and the inhibition was prevented by JD5037 (Fig. 1D). In cells with siRNA-mediated knockdown of *Sirt1*, insulin-induced Akt phosphorylation at ser473 was similar to that in mock-transfected controls (28), but the reversal of ACEA inhibition of the insulin response by CB_1R blockade was blunted (Fig. 1D). When *Rictor* was knocked down, insulin-induced Akt phosphorylation at ser473 was greatly suppressed and JD5037 failed to rescue it (Fig. 1D). Similar results were obtained in HepG2 cells (Supporting Fig. S1). Thus, Sirt1/mTORC2/Rictor signaling is required for the reversal of cannabinoid-mediated suppression of hepatic insulin signaling by CB_1R inverse agonists.

CB_1R BLOCKADE REVERSES HFD-INDUCED SUPPRESSION OF MTORC2 SIGNALING IN THE LIVER

We also monitored relative mTORC2 activity in the mouse liver *in vivo*, as reflected by mTOR ser2481 phosphorylation by immune-precipitated Rictor. Liver mTORC2 activation decreased in DIO compared to lean mice, and the decrease was reversed into an increase following daily treatment of DIO mice for 4 weeks with rimonabant or JD-5037. Similar high levels of $pmTOR_{ser2481}$ were detectable in the livers of HFD-fed $LCB_1R^{-/-}$ mice in the absence of CB_1R antagonist treatment (Fig. 2A). The relative levels of *Rictor* mRNA (Fig. 2B) and protein (Fig. 2D) were similarly decreased in vehicle-treated DIO compared to lean mice but increased in DIO mice treated daily with rimonabant (5 mg/kg/day) or JD-5037 (3 mg/kg/day), or in untreated $LCB_1R^{-/-}$ mice on either STD or HFD. Thus, increased $mTOR_{ser2481}$ phosphorylation may be due to increased Rictor levels. Sirt1 enzyme activity (Fig. 2C) as well as the phosphorylation status of the mTORC2 downstream targets Akt_{ser473} and $FOXO1_{ser256}$ (Fig. 2D) showed the same pattern of changes. Together, these findings suggest that the mTORC2/Rictor/Akt/FOXO1 pathway mediates CB_1R-induced hepatic insulin resistance in DIO mice and its reversal by blockade or deletion of hepatic CB_1R.

REVERSAL OF HEPATIC INSULIN RESISTANCE BY CB_1R BLOCKADE IS SIRT1-DEPENDENT

Next, we examined whether the effect of JD-5037 on mTORC2/Rictor/Akt signaling is dependent on hepatic Sirt1. Two-week treatment with JD5037, 3 mg/kg/day, increased Sirt1 protein in the liver of HFD-fed wild-type mice, whereas Sirt1 was absent in the liver of Sirt1-LKO mice, although a minor aberrant protein with lower molecular weight was detectable (Supporting Fig. S2A). Sirt1-LKO mice were phenotypically normal under a chow diet, and the HFD-induced increase in body weight as well as its reversal by JD5037 treatment were similar in Sirt1-LKO mice and wild-type controls (Supporting Fig. S2B). Hepatic gluconeogenesis was assessed using the pyruvate tolerance test (ipPTT). The glucose response to ipPTT was markedly increased by HFD in both strains, and JD5037 treatment significantly reduced it in wild-type but not in Sirt1-LKO mice (Fig. 3A). Similarly, JD5037 treatment reversed the HFD-induced hyperinsulinemia in wild-type mice but caused only a small and statistically insignificant decrease in Sirt1-LKO mice (Fig. 3B). A similar, strain-dependent difference was noted in the ability of JD5037 treatment to reverse HFD-induced glucose intolerance, insulin resistance and fasting hyperglycemia (Supporting Fig. S3). Thus, the reversal of the HFD-induced hyperglycemia and insulin resistance by CB_1R blockade are hepatic Sirt1-dependent.

Hyperinsulinemic/euglycemic clamps were conducted to explore the tissue-dependent mechanism of these effects. HFD induced hepatic insulin resistance, as indicated by the decreased insulin-mediated suppression of hepatic glucose production, which was completely normalized by JD5037 treatment in wild-type but not in Sirt1-LKO mice (Fig. 3C). JD5037 treatment also normalized the HFD-induced reduction of whole-body glucose disposal rate (Rd) and glucose infusion rate (GIR) in wild-type mice but not in Sirt1-LKO mice. Furthermore, glucose uptake in muscle and fat tissues, as revealed by 2-deoxyglucose uptake, were increased by JD5037 in wild-type but not Sirt1-LKO mice (Fig. 3D). A hepatic Sirt1-dependent increase in hepatic glucose storage may also contribute to the reversal of hyperglycemia by JD5037 in wild-type mice (Fig. 3E). JD-5037 treatment of DIO mice also normalized the reduced *Rictor* mRNA and protein expression and the reduced Akt phosphorylation in the liver of wild-type, but not Sirt1-LKO mice (Fig. 3F). *CB_1R* mRNA expression in liver, skeletal muscle and adipose tissue were similar in wild-type and Sirt1-LKO mice (data not shown), indicating that the absence of responses to JD5037 in the latter was not due to reduced CB_1R expression.

CB_1R BLOCKADE REDUCES MITOCHONDRIAL ROS PRODUCTION IN DIO MICE VIA HEPATIC SIRT1

HFD feeding promotes the accumulation of free fatty-acids in the liver, which is known to increase the reduction pressure on the mitochondrial respiratory chain, increase ROS production, and impair mitochondrial function (29). Sirt1 protects against HFD-induced metabolic damage through the induction of antioxidant proteins (30), and complete deletion of Sirt1 in the liver leads to whole body insulin resistance. Accordingly, the HFD-induced elevation of 4-HNE, a marker of oxidative stress/lipid peroxidation, was significantly attenuated by JD5037 treatment in wild-type but not Sirt1-LKO mice in both liver (Fig. 4A) and epididymal fat (Fig. 4B). Consistently, the HFD-induced decrease in Akt

phosphorylation at ser473 in white adipose tissue was not restored by 2 weeks of JD5037 treatment in Sirt1-LKO mice, which may account for the inefficiency of glucose uptake in the peripheral tissue with unchanged Sirt1 expression (Fig. 3D). Liver mitochondrial respiratory complex (MRC) I activity was increased by HFD in both strains, which again, was normalized in wild-type but not Sirt1-LKO mice (Fig. 4C). Total antioxidant capacity in the circulation showed an age-dependent decrease in Sirt1-LKO, but not wild-type, mice (Fig. 4D). These data indicate that hepatic Sirt1 is critical for maintaining antioxidation processes and is required for JD5037 reversal of HFD-induced mitochondrial ROS production in the liver, which contributes to hepatic and, eventually, whole-body insulin resistance.

CB_1R Blockade Reverses HFD-Induced Steatosis and Increases Fatty Acid β-Oxidation Independently of Hepatic Sirt1

We next investigated the signaling pathways involved in the reversal of liver steatosis by peripheral CB_1R blockade. Sirt1-LKO mice and their wild-type littermates had similar hepatic triglyceride content on STD. HFD feeding for 18 weeks significantly increased hepatic triglycerides and plasma ALT levels in both strains. Although the rise in hepatic triglycerides was somewhat less in Sirt1-LKO than in WT mice, JD5037 treatment resulted in similar reversal of both changes in the two strains (Supporting Fig. S4), suggesting that these effects are independent from hepatic Sirt1.

Increased fatty-acid oxidation contributes to the reversal of steatosis by CB_1R blockade (9, 24). We quantified hepatic fatty-acid β-oxidation by incubating [^{14}C]oleic acid with fresh liver homogenates and measuring the total radioactivity recovered as CO_2 plus acid-soluble products, as described (31). The basal rate of fatty-acid β-oxidation in Sirt1-LKO mice on STD was ~25% lower than in wild-type littermates on STD ($P<0.05$). HFD suppressed fatty-acid β-oxidation in both groups, which was similarly reversed by JD5037 treatment to or above levels in the respective lean groups (Fig. 5A). Thus, hepatic Sirt1 contributes to fatty-acid β-oxidation in the liver, but its CB_1R-mediated suppression in DIO mice is independent of Sirt1. Indirect calorimetry further confirmed that JD5037 treatment selectively increased fat oxidation and total energy expenditure in the both strains (Fig. 5B and Supporting Fig. S5).

Consistently, JD5037 treatment activated AMPK, a major mediator of fatty-acid β-oxidation, to the same extent in the livers of HFD-fed Sirt1-LKO and control mice (Fig. 5C), and this was paralleled by similar increases in hepatic fatty acids, reversed by JD5037 treatment, in the two strains (Supporting Fig. S6). LKB1 encodes a serine-threonine kinase that directly phosphorylates and activates AMPK and we used HepG2 cells with *LKB1* gene knockdown to test its involvement in the effect of JD5037 on AMPK phosphorylation. In mock-transfected cells, JD5037 caused long-lasting AMPK activation, whereas siRNA knockdown of *LKB1* by 62.7% ± 8.1% resulted in marked suppression of Thr172 phosphorylation of AMPK and blunted the effect of JD5037 (Fig. 5D). Incubation of HepG2 cells with 100nM JD5037 or rimonabant significantly increased the rate of fatty acid oxidation, as measured by a cellular energy flux analysis, and these effects were also blunted in cells with *LKB1* knocked down (Fig. 5E).

CB_1R BLOCKADE DOES NOT AFFECT MTORC1 SIGNALING AND ITS MODULATION BY INSULIN

mTORC1 and its downstream target p70S6K exert a negative feedback on insulin signaling. We therefore tested whether mTORC1/p70S6K is involved in the modulation of insulin signaling by CB_1R. In agreement with earlier findings, JD-5037 treatment of DIO mice increased Rictor protein level and FOXO1 phosphorylation at ser256 in the livers of wild-type, but not Sirt1-LKO mice, whereas the phosphorylation status of $p70S6K_{T389}$ was similar in the livers of these two groups and it was unaffected by CB_1R inverse agonist treatment in both strains (Fig. 6A). In HepG2 cells, neither CB_1R agonists nor inverse agonists affected the phosphorylation status of mTORC1 or a number of its downstream targets (Fig. 6B). Thus, the mTORC1 pathway does not seem to be involved in the modulation of insulin signaling via CB_1R in obesity.

Discussion

Obesity is associated with an overactive endocannabinoid system, and selective blockade of CB_1R in peripheral tissues, including the liver, reverses HFD-induced metabolic abnormalities by restoring normal lipid and glucose homeostasis (7, 9). The evidence provided here implicates the nutrient sensors Sirt1, mTORC2 and AMPK in the beneficial metabolic effects of CB_1R blockade and establishes endocannabinoids as upstream regulators of these key pathways.

mTORC2 functions primarily as an effector of insulin/PI3K/Akt-2 signaling (11). Endocannabinoids acting via CB_1R mediate obesity-related hepatic insulin resistance by inhibiting insulin-induced Akt-2 phosphorylation, and this effect is abrogated by hepatocyte-specific deletion or pharmacologic blockade of CB_1R (4). The present findings indicate, for the first time, that hepatic CB_1R signal via the Sirt1/mTORC2 pathway to impair insulin sensitivity by downregulating both Sirt1 and Rictor, whereas peripheral CB_1R blockade reverses similar changes induced *in vivo* by a high-fat diet. Peripheral CB_1R blockade not only abrogated the HFD-induced suppression of Rictor and its downstream targets $pAkt_{ser473}$ and $pFOXO1_{ser256}$ in the liver but increased them well above their level in lean control mice (Fig. 2). This may be related to the inverse agonist properties of the antagonists used or may reflect the tonic activation of CB_1R even in the lean state, and the latter explanation is supported by similarly elevated gene expression levels of the same proteins in the liver of untreated $LCB1^{-/-}$ mice on STD (Fig. 2B). The finding that siRNA-mediated knockdown of *Sirt1* results in a parallel reduction in *Rictor* expression (Supporting Fig. S1C) is consistent with the proposed role of Sirt1 as a transcriptional regulator of *Rictor* (14). Finally, the key role of the Sirt1/mTORC2 pathway in mediating the insulin sensitizing effect of CB_1R blockade *in vivo* is supported by the results of insulin clamp experiments, which indicated that in Sirt1-LKO mice JD5037 lost its ability to reverse the diet-induced hepatic insulin resistance (Fig. 3C). Peripheral insulin resistance was also less effectively reversed by JD5037 in HFD-fed Sirt1-LKO compared to wild-type mice (Fig. 3C and D), even though Sirt1 is present in muscle and adipose tissue of the former. This may be because HFD increases ROS production, and circulating ROS can cause generalized damage to the mTORC2 pathway (14).

Obesity is associated with impaired mitochondrial function in the liver, which is reversed by CB_1R blockade (22), and previous findings implicated increased signaling via AMPK in the latter effects (19, 32). In the liver, mitochondrial respiratory chain deficiency plays a key role in the pathology of nonalcoholic steatohepatitis regardless its initial cause (33). An overactive endocannabinoid/CB_1R system was found to impair mitochondrial function by reducing its biogenesis (34, 35). Sirt1 has been shown to protect mice from HFD-induced mitochondrial damage through activation of antioxidant proteins (30). Our finding that ROS production in DIO mice, as indicated here by increased 4-HNE levels in the liver and white adipose tissue (Fig. 4A, B), was reduced by peripheral CB_1R blockade confirms the role of an overactive endocannabinoid/CB_1R system in increasing ROS production in obesity. Furthermore, the dependence of this effect on hepatic Sirt1 and the deterioration of the total antioxidant capacity in the circulation of aged Sirt1-LKO mice (Fig. 4D) indicate its critical role in activating antioxidants throughout peripheral tissues and, consequently, in mitigating insulin resistance.

We have earlier demonstrated that the **P**leckstrin **H**omology (PH) domain and **L**eucine-rich repeat **P**rotein **P**hosphatase **1** (PHLPP1), which directly dephosphorylates and inactivates Akt-2 (36), is a downstream target of CB_1R for inducing insulin resistance in DIO mice (4). mTORC2 and PHLPP1 have been recently identified as part of a regulatory complex for chaperone mediated autophagy (CMA) where they serve opposite – stimulatory and inhibitory - functions (37). The present findings suggest that a similar kinase/phosphatase complex of mTORC2 and PHLPP1 may be involved in the regulation of insulin sensitivity by CB_1R, activation of which downregulates Rictor and upregulates PHLPP1 expression. Overall, the above findings indicate that the Sirt1/mTORC2/Akt pathway is a critical target for CB_1R blockade in reversing obesity-induced insulin resistance.

mTORC1/p70S6K exerts a negative feedback on insulin signaling. It has been shown that Sirt1 serves as a negative regulator of UPR signaling in T2DM and improves metabolic parameters largely through the inhibition of mTORC1 and ER stress in a mouse model of Sirt1 overexpression in the liver (38). However, CB_1R blockade did not suppress p70S6K phosphorylation in the liver of HFD-fed control or Sirt1-LKO mice, nor did CB_1R agonists or antagonists affect insulin-induced mTORC1 signaling in HepG2 cells (Fig. 6), indicating that mTORC1 and its downstream targets are not involved in CB_1R signaling and its role in regulating insulin action.

Activation of hepatic CB_1R also promotes lipogenesis and inhibits lipolytic processes (3, 24). However, the CB_1R-induced increase in *de novo* lipogenesis makes only a minor contribution to HFD-induced steatosis, which is largely due to uptake and incorporation into triglycerides of free fatty acids released from adipose tissue, whereas reversal of hepatic steatosis by CB_1R blockade is due to increased lipolysis and fatty acid oxidation in the liver (9). These effects appear to be independent of hepatic Sirt1, as JD5037 treatment fully reversed the HFD-induced suppression of hepatic fatty acid oxidation in both wild-type and Sirt1-LKO mice (Fig. 5A), and the *in vivo* increase in fatty acid oxidation measured by indirect calorimetry was also similar in the two strains (Fig. 5B). Instead, activation of AMPK via LKB1, a key upstream regulator of the fatty acid β-oxidation pathway is likely

involved, as JD5037 treatment completely reversed the HFD-induced suppression of AMPK phosphorylation in both wild-type and Sirt1-LKO mouse liver (Fig. 5C).

In conclusion, peripheral CB_1R blockade improves hepatic insulin signaling and glycemic control in obese mice through activation of the Sirt1/mTORC2/Akt pathway. In contrast, the parallel increase in hepatic fatty acid oxidation is largely independent of Sirt1 and likely involves activation of AMPK as summarized schematically in Figure 7.

Supplementary Material

Refer to Web version on PubMed Central for supplementary material.

Acknowledgements

We thank Drs. Xiaoling Li for providing the Sirt1-LKO mice used in this study, and Dechun Feng for isolating primary mouse hepatocytes and performing H&E staining.

Funding: Supported by intramural funds from the National Institute on Alcohol Abuse and Alcoholism.

REFERENCES

1. Di Marzo V, Goparaju SK, Wang L, Liu J, Batkai S, Jarai Z, Fezza F, et al. Leptin-regulated endocannabinoids are involved in maintaining food intake. Nature 2001;410:822–825. [PubMed: 11298451]
2. Cota D, Marsicano G, Tschop M, Grubler Y, Flachskamm C, Schubert M, Auer D, et al. The endogenous cannabinoid system affects energy balance via central orexigenic drive and peripheral lipogenesis. J Clin Invest 2003;112:423–431. [PubMed: 12897210]
3. Osei-Hyiaman D, DePetrillo M, Pacher P, Liu J, Radaeva S, Batkai S, Harvey-White J, et al. Endocannabinoid activation at hepatic CB1 receptors stimulates fatty acid synthesis and contributes to diet-induced obesity. J Clin Invest 2005;115:1298–1305. [PubMed: 15864349]
4. Liu J, Zhou L, Xiong K, Godlewski G, Mukhopadhyay B, Tam J, Yin S, et al. Hepatic cannabinoid receptor-1 mediates diet-induced insulin resistance via inhibition of insulin signaling and clearance in mice. Gastroenterology 2012;142:1218–1228 [PubMed: 22307032]
5. Ravinet Trillou C, Arnone M, Delgorge C, Gonalons N, Keane P, Maffrand JP, Soubrie P. Anti-obesity effect of SR141716, a CB1 receptor antagonist, in diet-induced obese mice. Am J Physiol Regul Integr Comp Physiol 2003;284:R345–353. [PubMed: 12399252]
6. Despres JP, Golay A, Sjostrom L. Effects of rimonabant on metabolic risk factors in overweight patients with dyslipidemia. N Engl J Med 2005;353:2121–2134. [PubMed: 16291982]
7. Tam J, Cinar R, Liu J, Godlewski G, Wesley D, Jourdan T, Szanda G, et al. Peripheral cannabinoid-1 receptor inverse agonism reduces obesity by reversing leptin resistance. Cell Metab 2012;16:167–179. [PubMed: 22841573]
8. Cinar R, Godlewski G, Liu J, Tam J, Jourdan T, Mukhopadhyay B, Harvey-White J, et al. Hepatic cannabinoid-1 receptors mediate diet-induced insulin resistance by increasing de novo synthesis of long-chain ceramides. Hepatology 2014;59:143–153. [PubMed: 23832510]
9. Tam J, Vemuri VK, Liu J, Batkai S, Mukhopadhyay B, Godlewski G, Osei-Hyiaman D, et al. Peripheral CB1 cannabinoid receptor blockade improves cardiometabolic risk in mouse models of obesity. J Clin Invest 2010;120:2953–2966. [PubMed: 20664173]
10. Tam J, Szanda G, Drori A, Liu Z, Cinar R, Kashiwaya Y, Reitman ML, et al. Peripheral cannabinoid-1 receptor blockade restores hypothalamic leptin signaling. Mol Metab 2017;6:1113–1125. [PubMed: 29031713]
11. Saxton RA, Sabatini DM. mTOR Signaling in Growth, Metabolism, and Disease. Cell 2017;168:960–976. [PubMed: 28283069]

12. Sarbassov DD, Guertin DA, Ali SM, Sabatini DM. Phosphorylation and regulation of Akt/PKB by the rictor-mTOR complex. Science 2005;307:1098–1101. [PubMed: 15718470]
13. Hagiwara A, Cornu M, Cybulski N, Polak P, Betz C, Trapani F, Terracciano L, et al. Hepatic mTORC2 activates glycolysis and lipogenesis through Akt, glucokinase, and SREBP1c. Cell Metab 2012;15:725–738. [PubMed: 22521878]
14. Wang RH, Kim HS, Xiao C, Xu X, Gavrilova O, Deng CX. Hepatic Sirt1 deficiency in mice impairs mTorc2/Akt signaling and results in hyperglycemia, oxidative damage, and insulin resistance. J Clin Invest 2011;121:4477–4490. [PubMed: 21965330]
15. Guarente L Mitochondria - A nexus for aging, calorie restriction, and sirtuins? Cell 2008;132:171–176. [PubMed: 18243090]
16. Winder WW, Hardie DG. AMP-activated protein kinase, a metabolic master switch: possible roles in type 2 diabetes. Am J Physiol 1999;277:E1–10. [PubMed: 10409121]
17. Li Y, Xu S, Mihaylova MM, Zheng B, Hou X, Jiang B, Park O, et al. AMPK phosphorylates and inhibits SREBP activity to attenuate hepatic steatosis and atherosclerosis in diet-induced insulin-resistant mice. Cell Metabolism 2011;13:376–388. [PubMed: 21459323]
18. Viollet B, Guigas B, Leclerc J, Hebrard S, Lantier L, Mounier R, Andreelli F, et al. AMP-activated protein kinase in the regulation of hepatic energy metabolism: from physiology to therapeutic perspectives. Acta Physiol (Oxf) 2009;196:81–98. [PubMed: 19245656]
19. Kola B, Hubina E, Tucci SA, Kirkham TC, Garcia EA, Mitchell SE, Williams LM, et al. Cannabinoids and ghrelin have both central and peripheral metabolic and cardiac effects via AMP-activated protein kinase. J Biol Chem 2005;280:25196–25201. [PubMed: 15899896]
20. Wu HM, Yang YM, Kim SG. Rimonabant, a cannabinoid receptor type 1 inverse agonist, inhibits hepatocyte lipogenesis by activating liver kinase B1 and AMP-activated protein kinase axis downstream of Galpha i/o inhibition. Molecular Pharmacology 2011;80:859–869. [PubMed: 21803969]
21. Jourdan T, Djaouti L, Demizieux L, Gresti J, Verges B, Degrace P. CB1 antagonism exerts specific molecular effects on visceral and subcutaneous fat and reverses liver steatosis in diet-induced obese mice. Diabetes 2010;59:926–934. [PubMed: 20110567]
22. Flamment M, Gueguen N, Wetterwald C, Simard G, Malthiery Y, Ducluzeau PH. Effects of the cannabinoid CB1 antagonist rimonabant on hepatic mitochondrial function in rats fed a high-fat diet. Am J Physiol Endocrinol Metab 2009;297:E1162–1170. [PubMed: 19724020]
23. Jourdan T, Demizieux L, Gresti J, Djaouti L, Gaba L, Verges B, Degrace P. Antagonism of peripheral hepatic cannabinoid receptor-1 improves liver lipid metabolism in mice: evidence from cultured explants. Hepatology 2012;55:790–799. [PubMed: 21987372]
24. Osei-Hyiaman D, Liu J, Zhou L, Godlewski G, Harvey-White J, Jeong WI, Batkai S, et al. Hepatic CB(1) receptor is required for development of diet-induced steatosis, dyslipidemia, and insulin and leptin resistance in mice. J Clin Invest 2008;118:3160–3169. [PubMed: 18677409]
25. Purushotham A, Schug TT, Xu Q, Surapureddi S, Guo X, Li X. Hepatocyte-specific deletion of SIRT1 alters fatty acid metabolism and results in hepatic steatosis and inflammation. Cell Metab 2009;9:327–338. [PubMed: 19356714]
26. Chorvat RJ, Berbaum J, Seriacki K, McElroy JF. JD-5006 and JD-5037: peripherally restricted (PR) cannabinoid-1 receptor blockers related to SLV-319 (Ibipinabant) as metabolic disorder therapeutics devoid of CNS liabilities. Bioorg Med Chem Lett 2012;22:6173–6180. [PubMed: 22959249]
27. Lamming DW, Ye L, Katajisto P, Goncalves MD, Saitoh M, Stevens DM, Davis JG, et al. Rapamycin-Induced Insulin Resistance Is Mediated by mTORC2 Loss and Uncoupled from Longevity. Science 2012;335:1638–1643. [PubMed: 22461615]
28. Li X SIRT1 and energy metabolism. Acta Biochim Biophys Sin (Shanghai) 2013;45:51–60. [PubMed: 23257294]
29. Lowell BB, Shulman GI. Mitochondrial dysfunction and type 2 diabetes. Science 2005;307:384–387. [PubMed: 15662004]
30. Pfluger PT, Herranz D, Velasco-Miguel S, Serrano M, Tschop MH. Sirt1 protects against high-fat diet-induced metabolic damage. Proc Natl Acad Sci U S A 2008;105:9793–9798. [PubMed: 18599449]

31. Demizieux L, Degrace P, Gresti J, Loreau O, Noel JP, Chardigny JM, Sebedio JL, et al. Conjugated linoleic acid isomers in mitochondria: evidence for an alteration of fatty acid oxidation. J Lipid Res 2002;43:2112–2122. [PubMed: 12454273]

32. Silvestri C, Di Marzo V. The Endocannabinoid System in Energy Homeostasis and the Etiopathology of Metabolic Disorders. Cell Metabolism 2013;17:475–490. [PubMed: 23562074]

33. Begriche K, Massart J, Robin MA, Bonnet F, Fromenty B. Mitochondrial Adaptations and Dysfunctions in Nonalcoholic Fatty Liver Disease. Hepatology 2013;58:1497–1507. [PubMed: 23299992]

34. Tedesco L, Valerio A, Cervino C, Cardile A, Pagano C, Vettor R, Pasquali R, et al. Cannabinoid type 1 receptor blockade promotes mitochondrial biogenesis through endothelial nitric oxide synthase expression in white adipocytes. Diabetes 2008;57:2028–2036. [PubMed: 18477809]

35. Tedesco L, Valerio A, Dossena M, Cardile A, Ragni M, Pagano C, Pagotto U, et al. Cannabinoid Receptor Stimulation Impairs Mitochondrial Biogenesis in Mouse White Adipose Tissue, Muscle, and Liver The Role of eNOS, p38 MAPK, and AMPK Pathways. Diabetes 2010;59:2826–2836. [PubMed: 20739683]

36. Grzechnik AT, Newton AC. PHLPPing through history: a decade in the life of PHLPP phosphatases. Biochem Soc Trans 2016;44:1675–1682. [PubMed: 27913677]

37. Arias E, Koga H, Diaz A, Mocholi E, Patel B, Cuervo AM. Lysosomal mTORC2/PHLPP1/Akt Regulate Chaperone-Mediated Autophagy. Mol Cell 2015;59:270–284. [PubMed: 26118642]

38. Li Y, Xu S, Giles A, Nakamura K, Lee JW, Hou X, Donmez G, et al. Hepatic overexpression of SIRT1 in mice attenuates endoplasmic reticulum stress and insulin resistance in the liver. FASEB J 2011;25:1664–1679. [PubMed: 21321189]

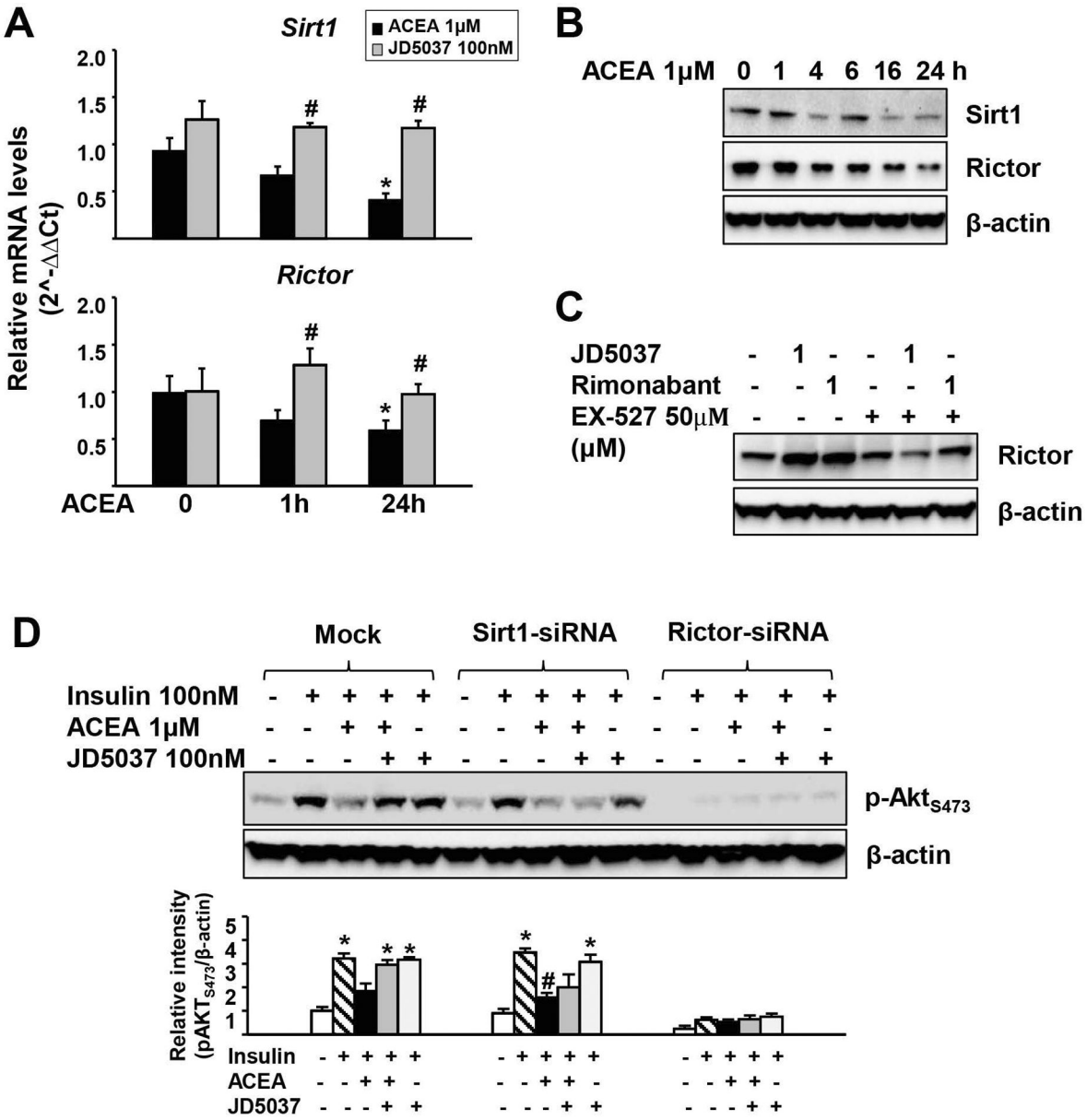

FIG. 1.

Activation of CB_1R inhibits Sirt1/mTORC2 signaling in mouse primary hepatocytes. **(A)** Effects of ACEA on *Sirt1* and *Rictor* expression. Primary mouse hepatocytes were incubated with DMSO or 100nM JD5037 for a total of 25h in the presence or absence of 1μM ACEA for the indicated time. Data represent mean ± SEM, *P<0.05 compared to vehicle-treated control (0 h); $^{\#}P$<0.05 compared to ACEA alone group. **(B)** Time-dependent effect of ACEA on Sirt1 and Rictor protein levels**. (C)** Effect of Sirt1 inhibitor EX-527 on CB_1R antagonist-induced increase in Rictor levels. **(D)** CB_1R blockade reverses ACEA-suppression of insulin signaling in primary hepatocytes in a Sirt1-dependent manner. Relative intensity of the bands was quantified using ImageJ software (NIH, Bethesda, MD) and normalized to β-actin levels. All representative data were repeated 3 times for statistical

analyses, as shown in the bar graph. Data represent mean ± SEM, *P<0.05 compared to vehicle-treated control; $^{\#}P$<0.05 compared to insulin alone group.

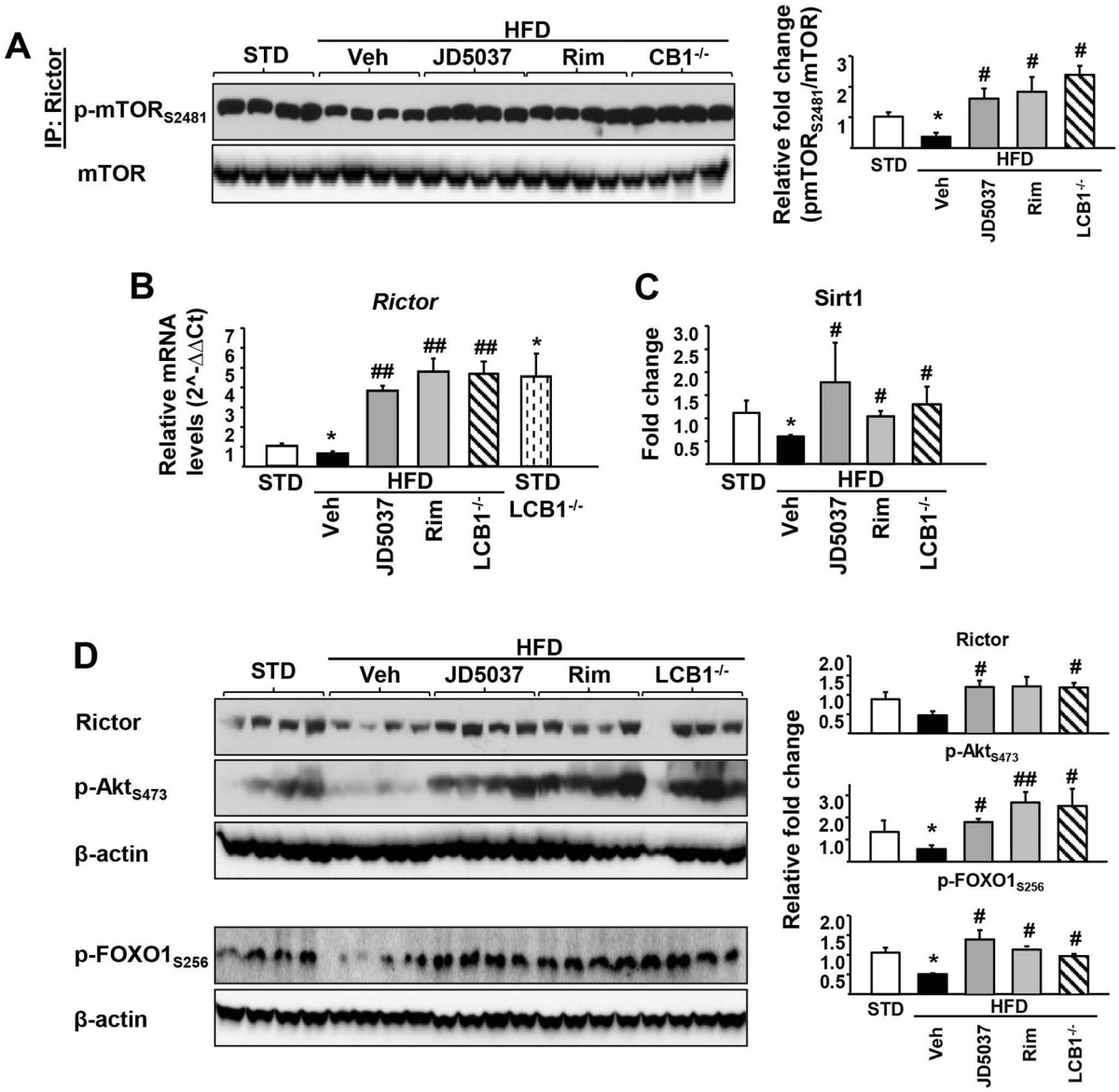

FIG. 2.

CB_1R blockade restores HFD-suppressed Sirt1/mTORC2 signaling in mouse liver. Pharmacologic blockade or genetic deletion of CB_1R reverses/prevents HFD-induced decrease in mTORC2 phosphorylation **(A),** *Rictor* gene expression (**B)** and Sirt1 activity **(C)** in the liver of DIO mice. The HFD-induced reductions in Rictor and the phosphorylation of its downstream targets Akt and FOXO1 are restored by CB_1R blockade **(D)**. Data represent mean ± SEM, $^{*}P<0.05$ compared to STD control group; $^{\#}P<0.05$ or $^{\#\#}P<0.001$ compared to HFD vehicle group. n=6–8/group.

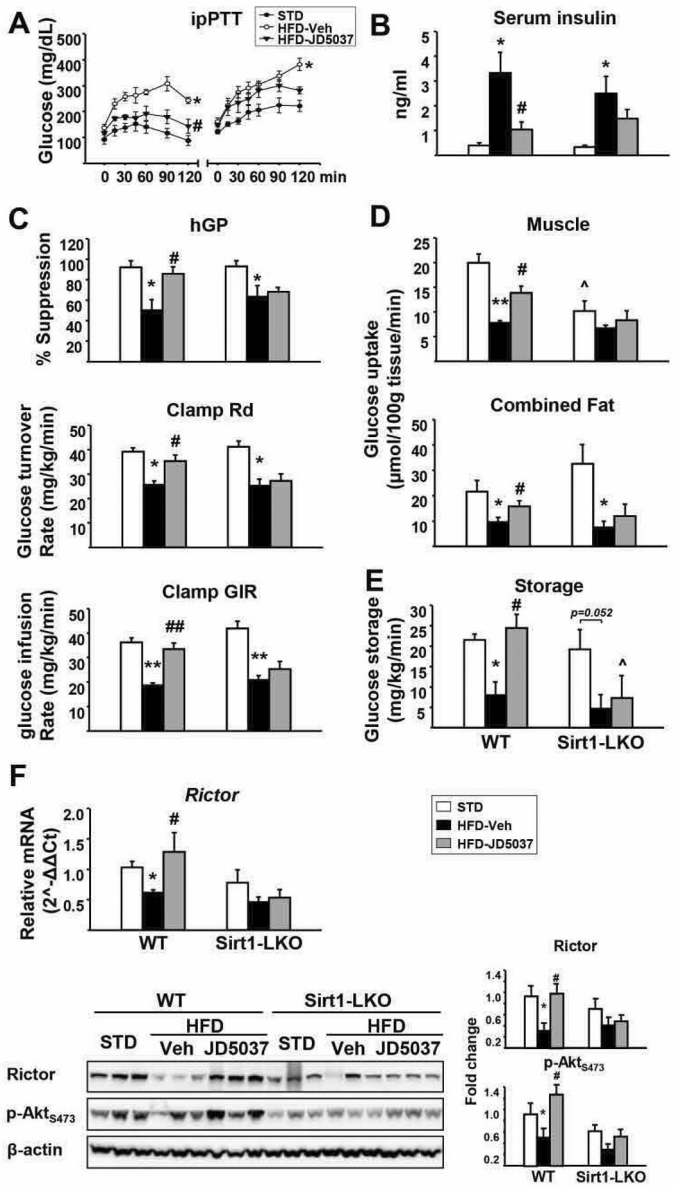

FIG. 3.

Hepatic Sirt1 is required for reversal of HFD-induced insulin resistance by JD5037.

(A) Effects of chronic JD5037 treatment on glucose metabolism as quantified by ipPTT. (**B)** Serum insulin levels in HFD-fed WT littermate and Sirt1-LKO mice. **(C)** Hyperinsulinemic/euglycemic clamps were performed in conscious, unrestrained WT and Sirt1-LKO mice as described in Supplementary Methods. Hepatic glucose production (hGP), whole body glucose clearance (Rd), and glucose infusion rates (GIR) during euglycemic insulin clamps. **(D)**, glucose uptake into gastrocnemius muscle and adipose tissues traced by 2-deoxy-d-[1-^{14}C] glucose at the end of insulin clamp and glucose storage **(E)** were measured. Values are mean ± SEM from n= 4–8 mice. *P<0.05, and **P< 0.001 compared to STD controls; $^{\#}P$<0.05, $^{\#\#}P$<0.001 compared to HFD vehicle group; $^{\wedge}P$<0.05 compared to the value from the same treatment group in WT mice. **(F)** HFD-induced decrease in *Rictor* gene expression

and protein level and $pAkt_{s473}$ are reversed by JD5037 treatment in the liver of WT but not Sirt1-LKO mice (quantified by densitometry using ImageJ software, $^{*}P<0.05$ compared to STD, $^{\#}P<0.05$ compared to HFD group). Data are representative of 4–5 mice in each group and repeated 3 times.

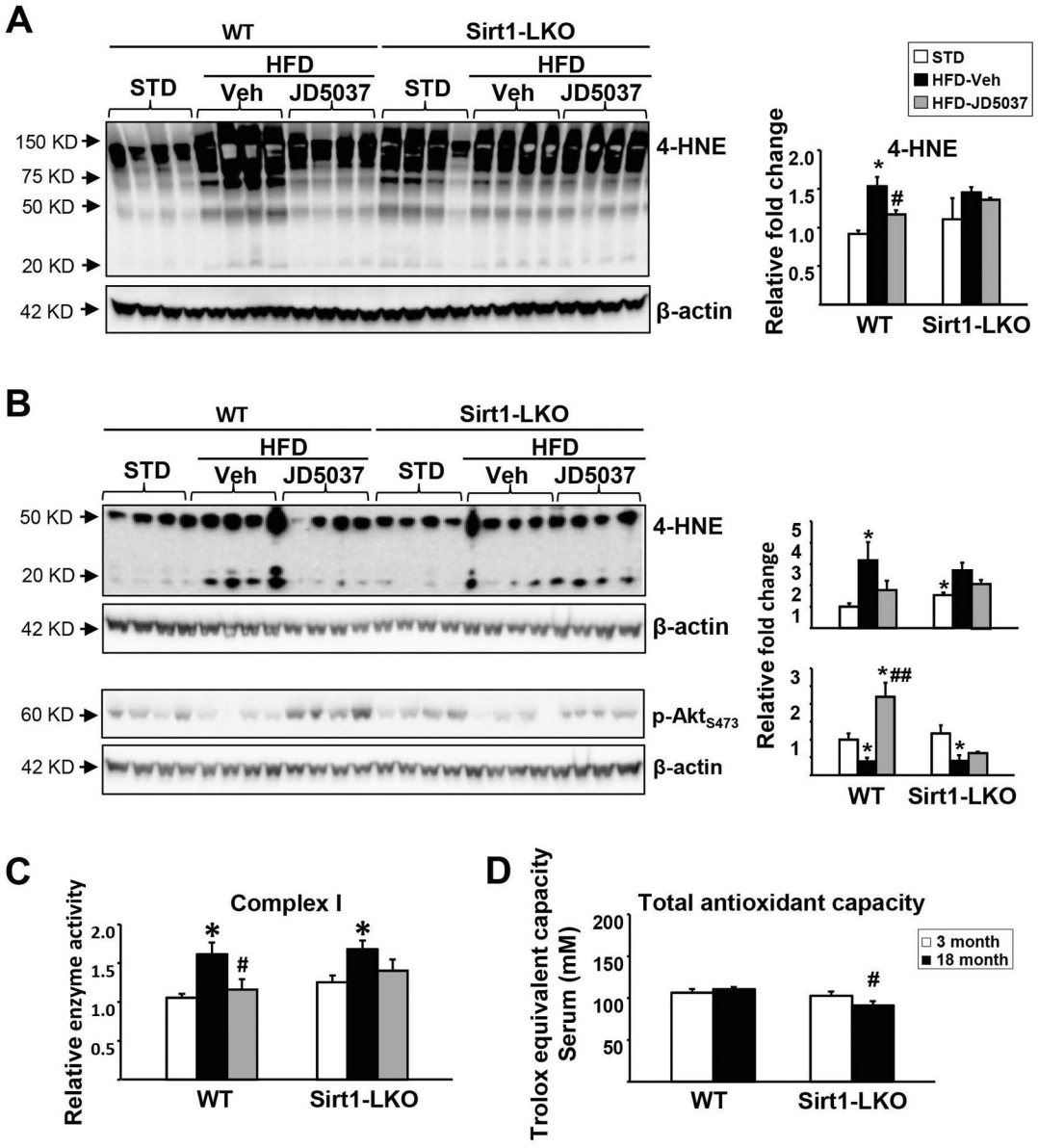

FIG. 4.

Effects of CB_1R blockade on HFD-induced oxidative stress and mitochondrial disfunction in WT and Sirt1-LKO mice.

JD5037 reversed HFD-induced mitochondrial ROS production, as indicated by 4-HNE adducts in liver **(A)** and white adipose tissue **(B)** in WT but not Sirt1-LKO mice. Same pattern observed for JD5037 reversal of $pAkt_{s473}$ in adipose tissue **(B)**. Western blot bands were quantified and analyzed by densitometry as indicate above. (**C)** Mitochondrial complex I activity was measured in freshly prepared liver mitochondria as described in Supplementary Methods. **(D)** Total antioxidant capacity was measured in serum. Data are mean ± SEM, n=5. *p<0.05 compared to STD group, $^{\#}p$<0.05 compared to HFD Veh group, or same age group in (D).

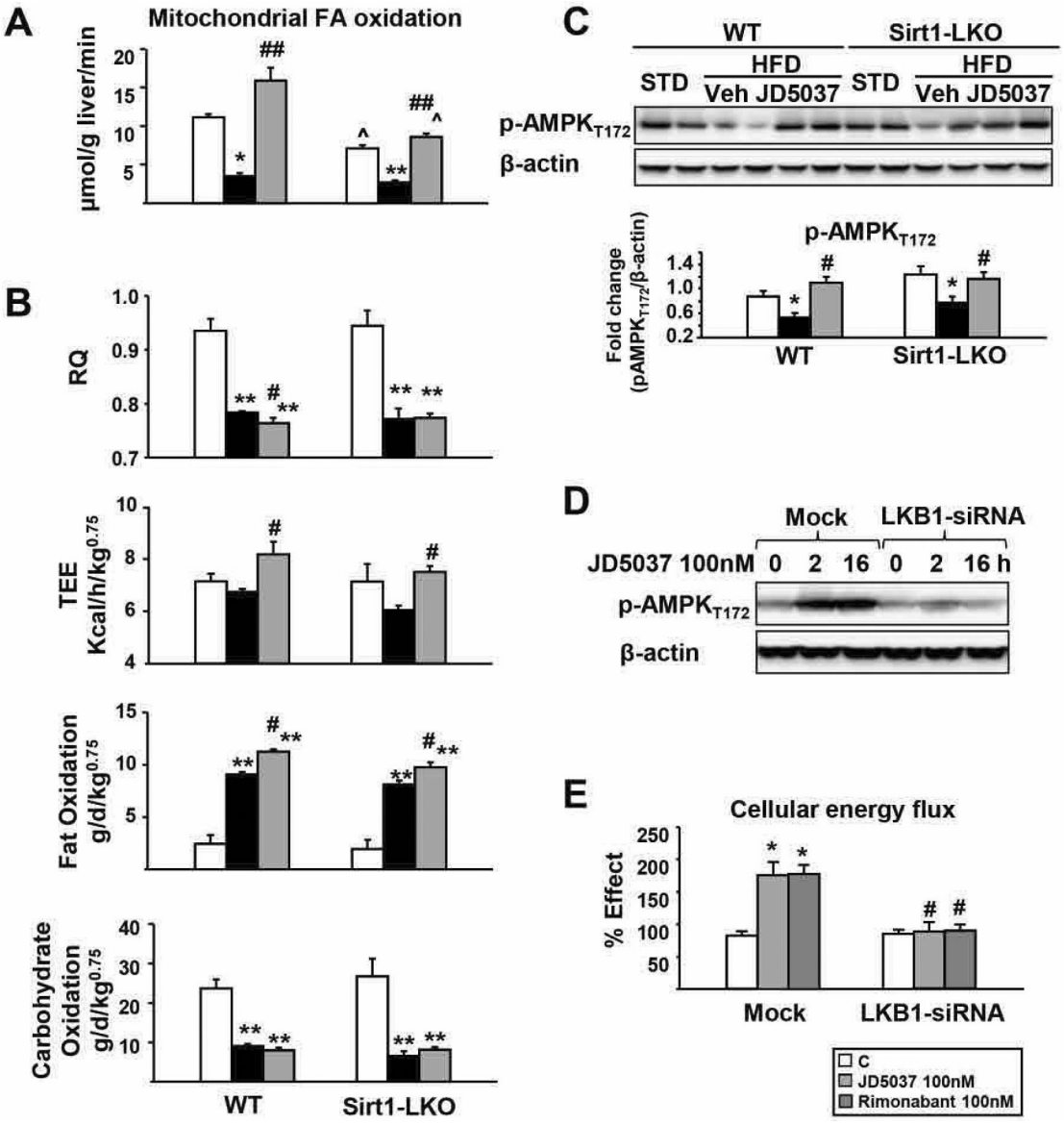

FIG. 5.

Reversal of HFD-induced decrease in hepatic fatty acid oxidation and AMPK phosphorylation by CB_1R blockade is independent of hepatic Sirt1.

(A) Rate of fatty acid β-oxidation in mitochondria from freshly prepared liver homogenates incubated with [^{14}C]oleic acid, as measured by the radioactivity recovered as CO_2 plus acid-soluble products **(B)** ***in vivo*** respiratory quotient (RQ), total energy expenditure and fatty acid and carbohydrate oxidation rates determined by indirect calorimetry over a 24 h period; **(C)** effects of HFD and JD5037 treatment on hepatic AMPK phosphorylation in WT and Sirt1-LKO mice. n= 4 mice/group. Repeated at least three times. Densitometry as above. *p<0.05 and **p<0.001 compared to STD controls. $^{\#}p$<0.05, $^{\#\#}p$<0.001 compared to HFD vehicle group. $^{\wedge}p$<0.05 compared to the value from the same treatment group in WT mice. Inverse CB_1R antagonist activated AMPK **(D)** and increased fatty acid oxidation rate **(E)** through LKB1 in mock-transfected control but not in LKB1-siRNA-transfected HepG2

cells. Fatty acid oxidation complete assay was performed using a fluorescence kit from Abcam.

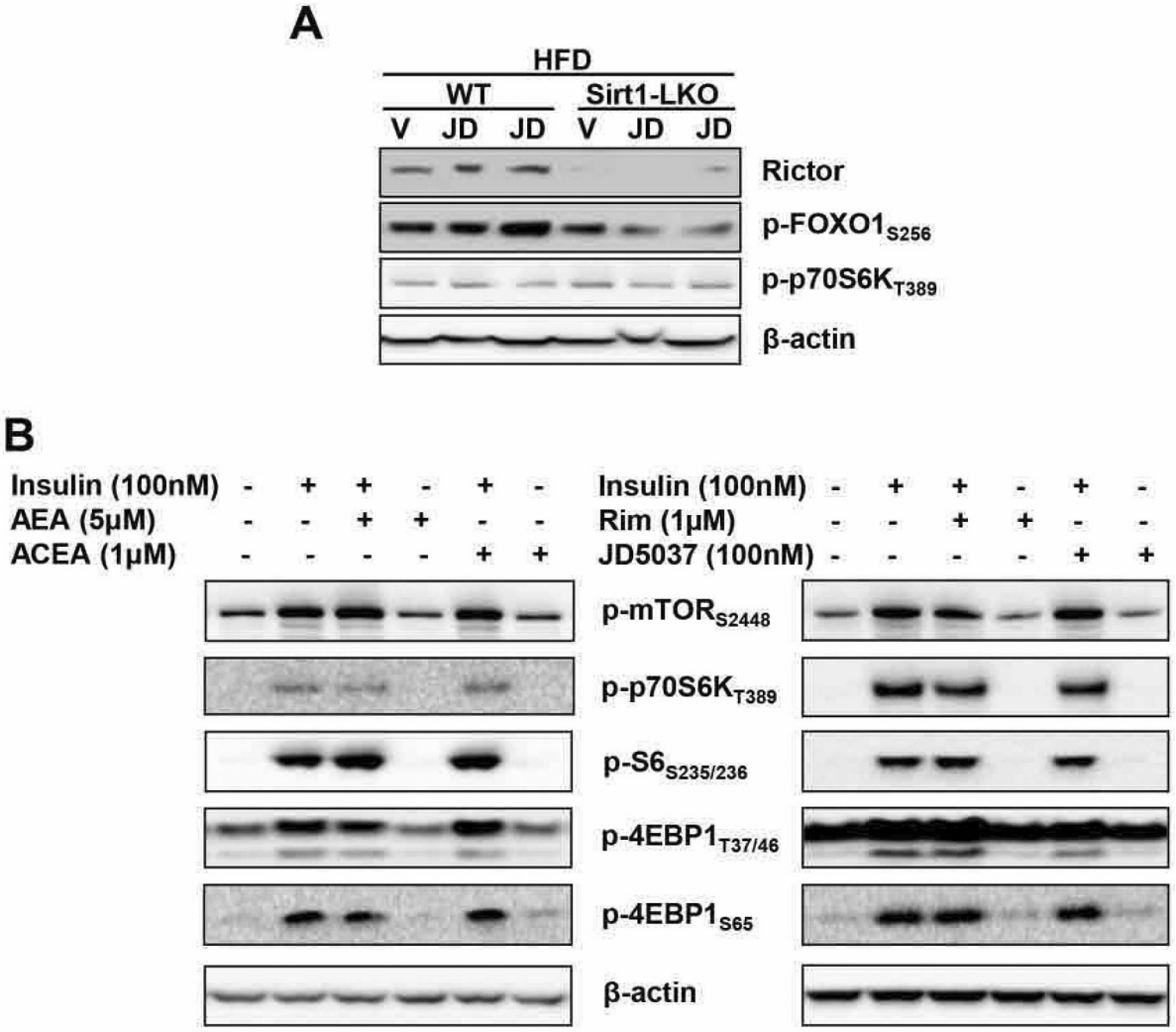

FIG. 6.

Lack of interaction between the hepatic CB_1R and mTORC1/p70S6K signaling systems. **(A)** Effects of JD5037 treatment (3 mg/kg/day for 2 weeks) of HFD-fed wild-type and Sirt1-LKO mice on hepatic Rictor protein, ser256 phosphorylation of the Rictor target FOXO1, and thr389 phosphorylation of the mTORC1 target p70S6K; (B**)** Lack of effects of CB1R agonists or inverse agonists on insulin induced phosphorylation of mTORC1 and its downstream targets in HepG2 cells.

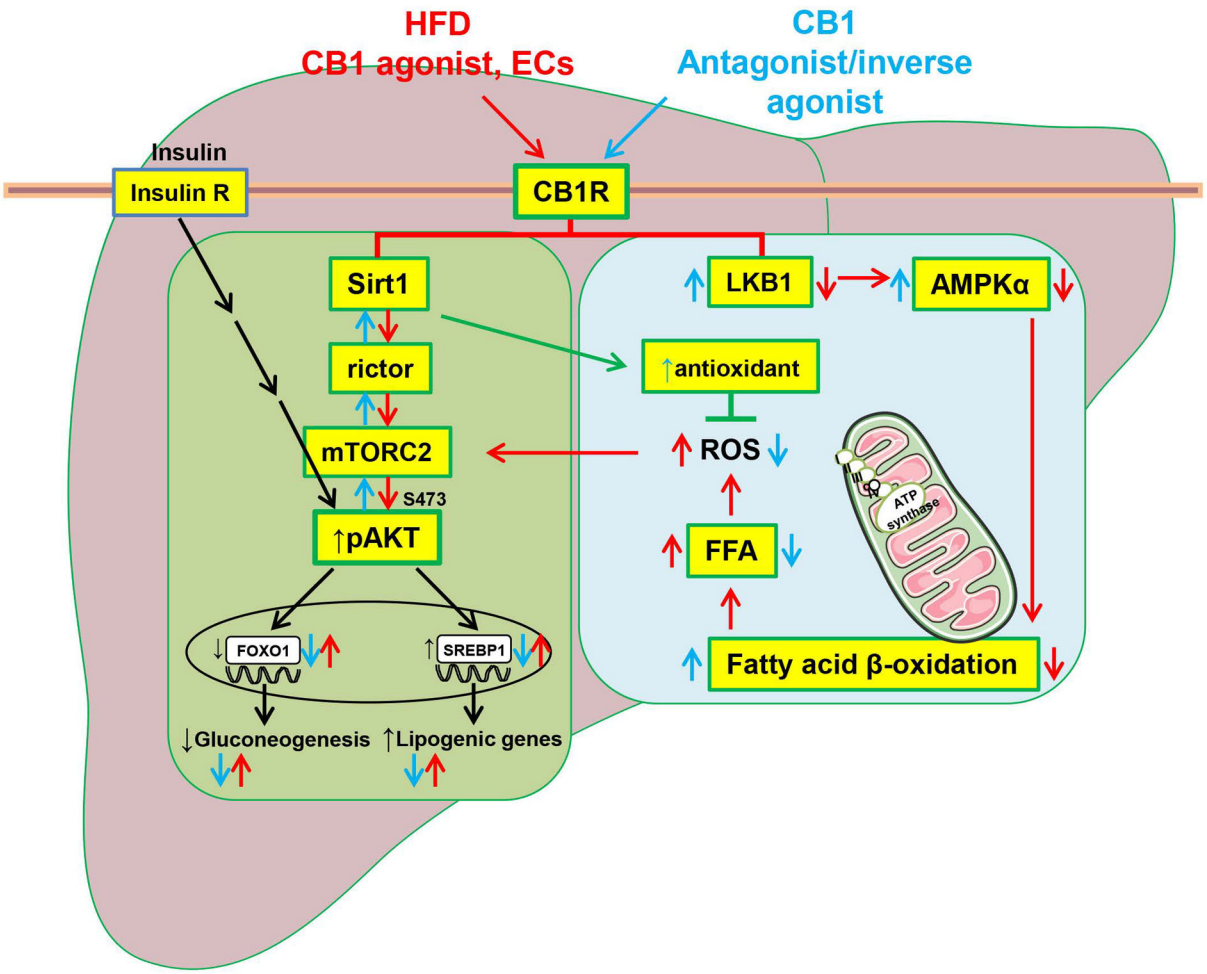

FIG. 7.

Schematic representation of the mechanism by which peripheral CB_1R blockade improves glucose and lipid metabolism through Sirt1/mTORC2 and LKB1/AMPK signaling, respectively.

We have shown earlier that both HFD and CB_1R agonist treatment inhibit hepatic insulin signaling via CB_1R-induced ER stress response through serine-307 phosphorylation of IRS1 and activation of Phlpp1 (4). New evidence illustrated here indicates that blockade of peripheral CB_1R reverses the HFD-induced, endocannabinoid-mediated impairment of insulin signaling by activating the Sirt1/mTORC2/Akt/FOXO1 pathway, whereas it reverses HFD-induced hepatic steatosis by increasing fatty acid oxidation via Sirt1-independent, LKB1-dependent activation of AMPK. Cross-talk between the two pathways may be mediated via ROS, production of which is promoted by HFD-induced increase in FFA, resulting in mitochondrial damage and inhibition of mTORC2 complex formation. Note that CB1R blockade restores insulin-suppression of hepatic glucose production but, unlike insulin, it also inhibits hepatic lipogenesis, as documented elsewhere (3). CB_1R agonist and antagonist effects are illustrated by red and blue arrows, respectively. Insulin effects are illustrated by black arrows.